

Laser-induced phase conversion of n-type $SnSe_2$ to p-type SnSe

Qi Zheng(郑琦), Rong Yang(杨蓉), Kang Wu(吴康), Xiao Lin(林晓), Shixuan Du(杜世萱), Chengmin Shen(申承民), Lihong Bao(鲍丽宏), and Hong-Jun Gao(高鸿钧)

Citation: Chin. Phys. B, 2022, 31 (**4**): 047306. DOI: 10.1088/1674-1056/ac4901
Journal homepage: http://cpb.iphy.ac.cn; http://iopscience.iop.org/cpb

What follows is a list of articles you may be interested in

Scaling dependence of memory windows and different carrier charging behaviors in Si nanocrystal nonvolatile memory devices

Jie Yu(于杰), Kun-ji Chen(陈坤基), Zhong-yuan Ma(马忠元), Xin-xin Zhang(张鑫鑫), Xiao-fan Jiang(江小帆), Yang-qing Wu(吴仰晴), Xin-fan Huang(黄信凡), Shunri Oda

Chin. Phys. B, 2016, 25 (**9**): 097304. DOI: 10.1088/1674-1056/25/9/097304

Electronic properties of the SnSe-metal contacts: First-principles study

Dai Xian-Qi, Wang Xiao-Long, Li Wei, Wang Tian-Xing

Chin. Phys. B, 2015, 24 (**11**): 117308. DOI: 10.1088/1674-1056/24/11/117308

Enhanced ultraviolet photoresponse based on ZnO nanocrystals/Pt bilayer nanostructure

Tong Xiao-Lin, Xia Xiao-Zhi, Li Qing-Xia

Chin. Phys. B, 2015, 24 (**6**): 067306. DOI: 10.1088/1674-1056/24/6/067306

Different charging behaviors between electrons and holes in Si nanocrystals embedded in SiN_x matrix by the influence of near-interface oxide traps

Fang Zhong-Hui, Jiang Xiao-Fan, Chen Kun-Ji, Wang Yue-Fei, Li Wei, Xu Jun

Chin. Phys. B, 2015, 24 (**1**): 017305. DOI: 10.1088/1674-1056/24/1/017305

Forward and reverse electron transport properties across a CdS/Si multi-interface nanoheterojunction

Li Yong, Wang Ling-Li, Wang Xiao-Bo, Yan Ling-Ling, Su Li-Xia, Tian Yong-Tao, Li Xin-Jian

Chin. Phys. B, 2014, 23 (**8**): 087307. DOI: 10.1088/1674-1056/23/8/087307

RAPID COMMUNICATION

Laser-induced phase conversion of n-type $SnSe_2$ to p-type SnSe

Qi Zheng(郑琦)[1,2,†], Rong Yang(杨蓉)[1,2,4,†], Kang Wu(吴康)[1,2], Xiao Lin(林晓)[2,3], Shixuan Du(杜世萱)[1,2,3,4], Chengmin Shen(申承民)[1,2,3], Lihong Bao(鲍丽宏)[1,2,3,4,‡], and Hong-Jun Gao(高鸿钧)[1,2,3,4,§]

[1] *Beijing National Center for Condensed Matter Physics and Institute of Physics, Chinese Academy of Sciences, Beijing* 100190, *China*
[2] *School of Physical Sciences, University of Chinese Academy of Sciences, Beijing* 100190, *China*
[3] *CAS Center for Excellence in Topological Quantum Computation, University of Chinese Academy of Sciences, Beijing* 100190, *China*
[4] *Songshan Lake Materials Laboratory, Dongguan* 523808, *China*

(Received 25 October 2021; revised manuscript received 6 January 2022; accepted manuscript online 7 January 2022)

We report a facile phase conversion method that can locally convert n-type $SnSe_2$ into p-type SnSe by direct laser irradiation. Raman spectra of $SnSe_2$ flakes before and after laser irradiation confirm the phase conversion of $SnSe_2$ to SnSe. By performing the laser irradiation on $SnSe_2$ flakes at different temperatures, it is found that laser heating effect induces the removal of Se atoms from $SnSe_2$ and results in the phase conversion of $SnSe_2$ to SnSe. Lattice-revolved transmission electron microscope images of $SnSe_2$ flakes before and after laser irradiation further confirm such conversion. By selective laser irradiation on $SnSe_2$ flakes, a pattern with $SnSe_2$/SnSe heteostructures is created. This indicates that the laser induced phase conversion technique has relatively high spatial resolution and enables the creation of micron-sized in-plane p–n junction at predefined region.

Keywords: $SnSe_2$, SnSe, laser irradiation, local phase conversion

PACS: 73.63.Bd, 64.70.Nd, 42.55.Ye, 78.30.−j **DOI:** 10.1088/1674-1056/ac4901

1. Introduction

In the past years, transition metal dichalcogenides (TMDs) have attracted intensive research interests due to their diverse electronic properties, such as metal/band insulators,[1–3] semiconductors,[3–7] charge density waves,[8–10] ferromagnetism,[11] valley polarization,[12,13] etc. These versatile properties come from the diversity of their compositions and phases, including trigonal prismatic (2H), octahedral (1T), rhombohedral (3R), monoclinic (1T′) phases,[14,15] etc. Due to the weak bonding energies in metal-selenium bonds, there is a low energy requirement to lose Se in selenide minerals and the phase transition in selenide minerals is widely reported.[16–18] Recently, an electron-beam induced phase conversion technique has been reported in which the electrons accelerated up to 300 keV in a transmission electron microscope (TEM) system gain enough energy for knocking a weak bonded atom (for example Se in $PdSe_2$)[19] out of the sample and the *in-situ* TEM observation provides the possibility of understanding the phase conversion mechanism in atomic scale. Besides the mechanism study, this local phase transition technique also provides high controllability to form semiconductor homojunction when the two phases before and after conversion have different properties, such as by converting n-type to p-type semiconductor, a p–n junction can be fabricated. Compared with the traditional nanomicro fabrication to prepare semiconductor p–n junctions by locally ion implantation, the local phase conversion technique is more efficient and has better controllability.

For the tin selenides, stable layered crystal phases (Fig. 1(a)) are known with Sn in Sn(IV) [$SnSe_2$, n-type] and Sn(II) [SnSe, p-type] oxidation states. The p–n junction of $SnSe_2$ and SnSe formed by local phase conversion of n-type $SnSe_2$ to p-type SnSe with *in-situ* electron beam irradiation in a TEM was firstly reported by P. Shutter *et al.* in 2016.[16] After that, thermally driven conversion of n-type $SnSe_2$ to p-type SnSe by direct heating is developed and in-plane p–n junction has been formed.[20] Creating in-plane p–n junctions at predefined locations is critical for further exploration of the novel properties and device applications of $SnSe_2$–SnSe heterostructure. Here, we report laser-induced transformations of layered tin dichalcogenides from n-type $SnSe_2$ to SnSe. By collecting Raman spectra on $SnSe_2$ flakes before and after laser irradiation, the phase conversion from n-type $SnSe_2$ to p-type SnSe is confirmed. The conversion mechanism of laser heating effect induced removal of Se atoms from $SnSe_2$ is revealed by the Raman spectra collected at different substrate temperatures and laser power levels. Lattice resolved transmission electron microscope (TEM) images confirms such conversion at atomic levels. Finally, a pattern with $SnSe_2$/SnSe heteostructures is created by selective laser irradiation on $SnSe_2$ flakes, indicating that the laser induced phase conversion technique

[†]These authors contributed equally.
[‡]Corresponding author. E-mail: lhbao@iphy.ac.cn
[§]Corresponding author. E-mail: hjgao@iphy.ac.cn

© 2022 Chinese Physical Society and IOP Publishing Ltd

has relatively high spatial resolution and enables the creation of micron-sized in-plane p–n junction at predefined region.

2. Methods

2.1. Growth of $SnSe_2$ nanoflakes

The $SnSe_2$ nanoflakes were grown by chemical vapor deposition (CVD) on a mica substrate using Se and SnI_2 pills as precursors,[21] as schematically shown in Fig. 1(a). The substrate was loaded into a double heating zone CVD furnace and placed 20 cm down steam to a quartz crucible containing 13.5 mg of SnI_2 ($\geqslant$ 99.999%, Alfa) with another quartz crucible containing 400 mg of Se ($\geqslant$ 99.999%, Alfa) in the upper steam. The Se pills in the first heating zone were heated up to 470 °C in advance to insure a Se rich environment. Then the SnI_2 pills were heated up to 530 °C in 10 min and kept for 15 min under a flow of 5 sccm $H_2 + 20$ sccm Ar carry gas. The key step to get thin and large $SnSe_2$ nanoflakes is fast cooling down the substrate to room temperature after the growth progress.

2.2. Sample characterization and laser irradiation progress

Optical microscope (BX51, OLMPUS) and atomic force microscope (SPA 400, SII) in tapping mode were used for characterization of the morphology and thickness of $SnSe_2$ flakes. TEM images and SAED pattern were taken by JEOL JEM-2100 at an accelerating voltage of 200 kV. TEM samples were prepared by directly scraping $SnSe_2$ flakes from the as grown substrate and collecting them on TEM grid. Laser irradiation on $SnSe_2$ flakes was performed by the laser in a confocal Raman/PL system (Horiba HR-Evolution) and the Raman spectra were collected *in-situ* before and after the phase conversion process. A home updated variable temperature (VT)-VACUUM Raman system (Horiba HR-800) was used for the temperature dependent conversion.

3. Results and discussion

3.1. Synthesis and characteristic of $SnSe_2$ nano flakes

The $SnSe_2$ flakes were synthesized by a CVD method.[21] Figures 1(b) and 1(d) show the optical micrograph of the as-grown $SnSe_2$ flakes. The $SnSe_2$ flakes show either hexagonal or triangular shapes, which can be controlled by varying the substrate temperature. As shown in Fig. 1(c), the lateral size of the triangular shaped flake can reach up to $\sim$ 80 μm. Its thickness was measured by line profile analysis of atomic force microscope (AFM). An AFM image of the $SnSe_2$ flake is shown in the inset of Fig. 1(c) and its thickness is measured as $\sim$ 2.1 nm. The lateral size of hexagonal $SnSe_2$ nano-flake can reach up to $\sim$ 30 μm (Fig. 1(e)). High-resolution transmission electron microscopy (HRTEM) was used to characterize the lattice structures of the $SnSe_2$ nanoflakes. The lattice fringes shown in Fig. 1(f) indicate a perfect atomic structure with a lattice spacing of 3.3 Å, corresponding to the $(10\bar{1})$ planes of a hexagonal-phase $SnSe_2$.[22] Further selected area electron diffraction (SAED) pattern also confirms the high quality and single-crystalline nature of $SnSe_2$, as shown in the inset of Fig. 1(f). The element analysis of Sn and Se by energy dispersive x-ray spectroscopy (EDX) study shows a 1 : 2 atomic ratio of Sn versus Se, as shown in Fig. S1. The Raman spectrum in Fig. 1(g) shows clear peaks of the E_g mode at 117 cm^{-1} and A_{1g} mode at 185 cm^{-1}, respectively, which is consistent with previous result.[23]

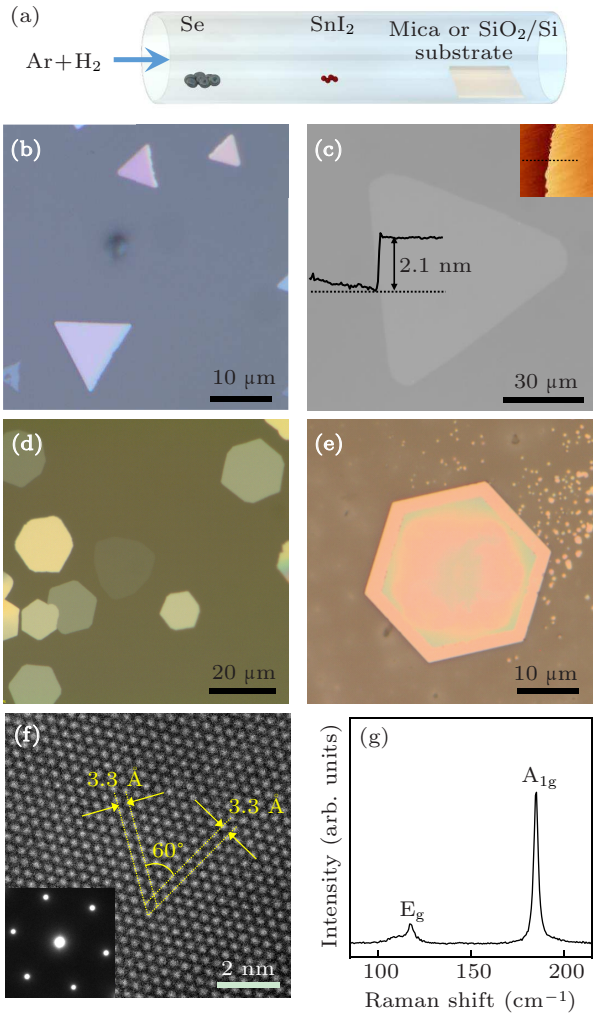


Fig. 1. Preparation and characterization of single crystalline $SnSe_2$ flakes. (a) Schematic diagram of the preparation of $SnSe_2$ flakes by CVD. (b) Optical image of triangular $SnSe_2$ flakes as-grown on a mica substrate. (c) Optical image of an individual $SnSe_2$ flake with thickness of 2.1 nm. Inset is the AFM image of the same $SnSe_2$ flake. (d) Optical image of hexagonal $SnSe_2$ flakes as-grown on a mica substrate. (e) Optical image of an individual $SnSe_2$ flake with hexagonal morphology. (f) Lattice-resolved TEM image of a single $SnSe_2$ nanoflake. Inset is the SAED image. (g) The Raman spectrum collected on a typical $SnSe_2$ nanoflake.

3.2. Laser induced conversion from $SnSe_2$ to SnSe

In Raman spectrum measurements, the Raman scatter signal increases with the gain of laser power and if high laser power is applied, the sample may be burnt by heating effect.

Figure 2(a) shows the burnt holes at top corner and right corner of a triangle $SnSe_2$ nanoflake after collecting Raman spectrum for 60 s with laser power of 25 mW under a 532 nm laser irradiation. To study the laser irradiation effect on the structure of $SnSe_2$ flake, Raman spectra were collected before and after the laser irradiation process. As shown in Fig. 2(b), the black line and red line represent the Raman signals before and after the laser irradiation progress, respectively, and the blue lines show the peaks fitting after the laser irradiation. In comparison to the Raman signal from $SnSe_2$, new Raman peaks located at 69 cm^{-1}, 93 cm^{-1} and 153 cm^{-1} emerge after the laser irradiation, which represents the A_g^1, B_{3g} and A_g^3 vibration modes of SnSe crystal,[24] respectively. This indicates that by laser irradiation on $SnSe_2$ flake, $SnSe_2$ can be converted to SnSe. In addition, the A_{1g} peak at 185 cm^{-1} and the E_g peak at 117 cm^{-1} of $SnSe_2$ remain after the laser irradiation, which indicates that $SnSe_2$ is not completely converted to SnSe. This is because that during laser irradiation the heat distribution of the irradiation area is not uniform. Figure 2(c) shows a simple sketch of the laser irradiation progress. The core part has a higher temperature than the edge of the outer area, so the conversion from $SnSe_2$ to SnSe may happen only in the core part. An AFM image of the burnt hole is shown in the upper inset of Fig. 2(c), which initially confirms that the laser heating effect might be the physical mechanism of the conversion. Furthermore, an area conversion progress is performed by point-by-point laser irradiation on $SnSe_2$ flake, as shown in Fig. 2(a). Figure 2(d) shows the Raman spectra collected from the area of original $SnSe_2$ (black), after point conversion (red) and after area conversion (blue), respectively. The green dashed rectangle highlights that the A_{1g} peak of $SnSe_2$ located at 185 cm^{-1} is substantially reduced after area conversion, indicating that the $SnSe_2$ is almost completely converted to SnSe.

3.3. The temperature- and laser power-dependent conversion of $SnSe_2$ to SnSe

To further study the conversion mechanism, temperature- and power-dependent conversion process was performed. To exclude the influence of the thickness of $SnSe_2$ on the conversion efficiency, a bulk $SnSe_2$ single crystal was used as the sample. As shown in Fig. 3(a), under a 532 nm laser irradiation, the Raman spectra collected on the region after conversion with different laser powers suggest that only the 15 mW irradiation can completely convert $SnSe_2$ to SnSe. Figure 3(b) shows the Raman spectra of $SnSe_2$ after conversion at different temperatures with a constant laser power of 15 mW. It is clearly found that the conversion can only happen at temperatures higher than 150 K. As a constant laser power has a constant heating effect, the conversion becomes impossible when the substrate is cooling down and even the hottest center area under the laser beam cannot gain enough energy to convert $SnSe_2$ to SnSe. A laser with longer wavelength of 633 nm was also used to convert $SnSe_2$ to SnSe. As shown in Fig. 3(c), only when the laser power reaches 8.3 mW, the conversion process can occur. For the conversion at different temperatures with constant power of 8.3 mW, the conversion process can

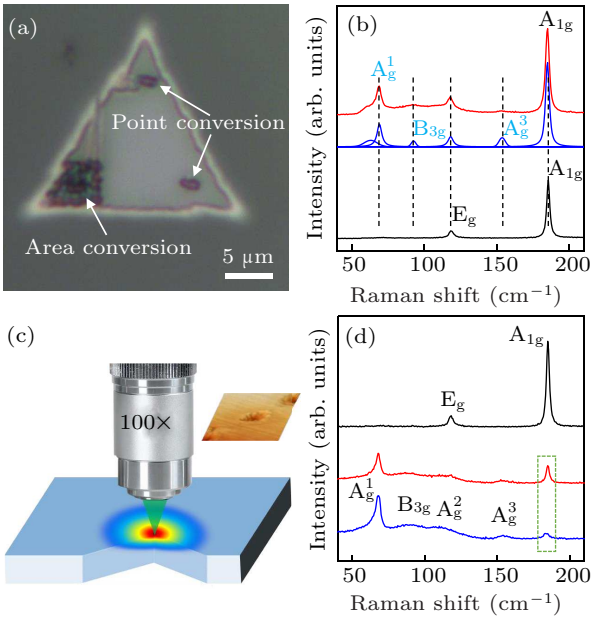


Fig. 2. Laser induced phase conversion of n-type $SnSe_2$ to p-type SnSe. (a) Optical microscope image of the $SnSe_2$ flake with point conversion and area conversion. (b) The Raman spectra before (black) and after (red) conversion together with peak fitting (blue). (c) The schematic diagram of the heat distribution during conversion and the 3D AFM image of a burnt hole (upper inset). (d) Raman spectra of original $SnSe_2$ (black), after point conversion (red) and area conversion (blue), respectively.

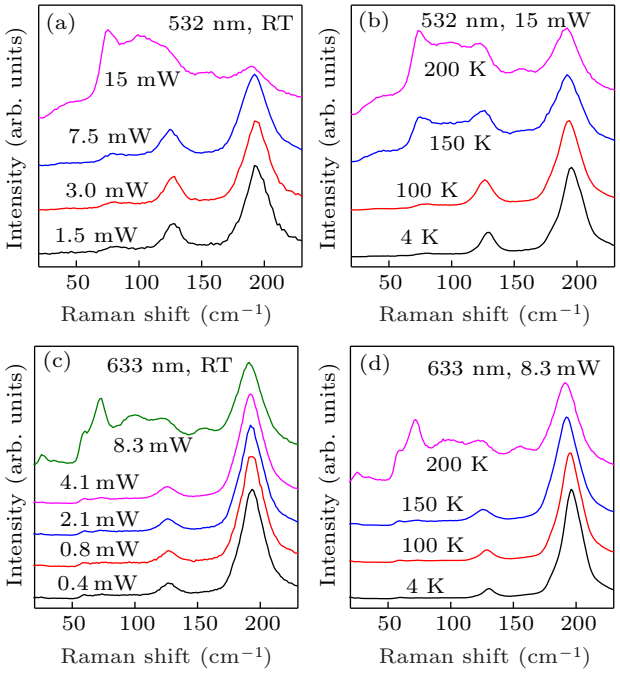


Fig. 3. Laser power- and temperature-dependent conversion of $SnSe_2$ to SnSe. (a) Raman spectra of $SnSe_2$ after a 532 nm laser irradiation with different laser powers at room temperature (RT). (b) Raman spectra of $SnSe_2$ after a 532 nm laser irradiation with power of 15 mW at different substrate temperatures. (c) Raman spectra of $SnSe_2$ after a 633 nm laser irradiation with different laser powers at RT. (d) Raman spectra of $SnSe_2$ after a 633 nm laser irradiation with power of 15 mW at different substrate temperatures.

only happen when the substrate temperature reaches 200 K. All these results confirm that the laser heating effect accounts for the physical mechanism of conversion of $SnSe_2$ to SnSe.

3.4. Patterned conversion of $SnSe_2$ to SnSe

HRTEM was used to further confirm that after laser irradiation, $SnSe_2$ is converted to SnSe. After laser irradiation, burnt holes with a diameter of 1–2 μm are clearly observed in the TEM image of $SnSe_2$ flake, as shown in Fig. 4(a). The lattice resolved HRTEM image of the the region at the edge of the burn hole after laser irradiation is shown in Fig. 4(b). The lattice fringes indicate a perfect atomic structure with a lattice spacing of 3.02 Å, corresponding to the $(0\bar{1}1)$ planes of a orthogonal-phase SnSe.[24] As discussed above, only the center region under laser irradiation can be converted. Therefore, the local conversion of $SnSe_2$ to SnSe at predefined regions can reach a higher spatial resolution than the laser spot. Figure 4(c) shows the AFM image of $SnSe_2$ flake after a 532 nm laser irradiation with power of 2 mW. The depth of burnt holes is $\sim$ 1.5 nm and the diameter is smaller than 200 nm, which is much smaller than the diameter of the laser spot ($\sim$ 500 nm) with the 100$\times$ objective lens. To demonstrate the capability of creation of in-plane $SnSe_2$–SnSe p–n junction by this local phase conversion technique, patterned conversion of $SnSe_2$ to SnSe was performed by point-by-point laser irradiation on $SnSe_2$ flakes. As shown in Fig. 4(d), an "IOP" pattern is clearly observed. Lower inset shows the Raman mapping at 69 cm^{-1} of the pattern, indicating that the irradiation area is completely converted into SnSe.

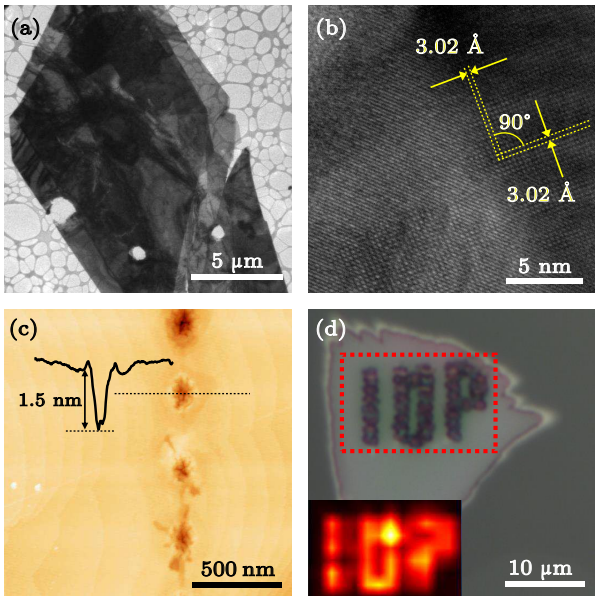


Fig. 4. (a) TEM image of the $SnSe_2$ flake after laser irradiation. Laser burnt holes can be clearly observed. (b) The lattice-resolved TEM image of the region at the edge of the burn hole after laser irradiation. (c) AFM image of $SnSe_2$ flake after a 532 nm laser irradiation with power of 2 mW. (d) Optical microscope image of $SnSe_2$ nanoflake after patterned laser-induced phase conversion. The lower inset shows the Raman mapping image of the pattern, indicating that the irradiation area is completely converted into SnSe.

4. Conclusion

In summary, we have developed a novel method to locally convert n-type $SnSe_2$ to p-type SnSe. This inversion is confirmed by collecting Raman spectra on $SnSe_2$ flakes before and after laser irradiation. The physical mechanism of this phase conversion is revealed by measuring the Raman spectra of $SnSe_2$ flakes after laser irradiation performed at different temperatures, indicating that it is the laser heating effect induces the removal of Se atoms from $SnSe_2$ to convert $SnSe_2$ to SnSe. High-resolution TEM image of $SnSe_2$ flakes after laser irradiation shows atomic structure of SnSe, further confirming the conversion of $SnSe_2$ to SnSe. The successful patterned conversion of $SnSe_2$ to SnSe shows that this laser induced phase conversion technique has a high spatial resolution better than the laser spot and enables the creation of micron-sized in-plane p–n junction at predefined region.

Acknowledgments

This work was supported by the National Key Research & Development Project of China (Grant Nos. 2016YFA0202300 and 2018FYA0305800), the National Natural Science Foundation of China (Grant No. 61888102), Strategic Priority Research Program of Chinese Academy of Sciences (Grant Nos. XDB30000000 and XDB28000000), and Youth Innovation Promotion Association of Chinese Academy of Sciences (Grant No. Y201902).

References

[1] Yu X, Cheng H, Zhang M, Zhao Y, Qu L and Shi G 2017 *Nat. Rev. Mater.* **2** 17046
[2] Wang J, Guo C, Guo W, Wang L, Shi W and Chen X 2019 *Chin. Phys. B* **28** 046802
[3] Zeng Y, Zhang S, Li X, Ao J, Sun Y, Liu W, Liu F, Gao P and Zhang Y 2019 *Chin. Phys. B* **28** 058101
[4] Novoselov K S, Geim A K, Morozov S V, Jiang D, Zhang Y, Dubonos S V, Grigorieva I V and Firsov A A 2004 *Science* **306** 666
[5] Cui X, Lee G H, Kim Y D, Arefe G, Huang P Y, Lee C H, Chenet D A, Zhang X, Wang L, Ye F, Pizzocchero F, Jessen B S, Watanabe K, Taniguchi T, Muller D A, Low T, Kim P and Hone J 2015 *Nat. Nanotechnol.* **10** 534
[6] Chu T, Ilatikhameneh H, Klimeck G, Rahman R and Chen Z 2015 *Nano Lett.* **15** 8000
[7] Zhou Z, Wu L, Chen J, Ma J, Huang Y, Shen C, Bao L and Gao H J 2020 *Chin. Phys. B* **29** 118501
[8] Zhu X Y, Wang S, Jia Z Y, Zhu L, Li Q Y, Zhao W M, Xue C L, Xu Y J, Ma Z, Wen J, Yu S L, Li J X and Li S C 2019 *Phys. Rev. Lett.* **123** 206405
[9] Altvater M A, Tilak N, Rao S, Li G, Won C J, Cheong S W and Andrei E Y 2021 *Nano Lett.* **21** 6132
[10] Song Z, Lei B, Cao Y, Qi J, Peng H, Wang Q, Huang L, Lu H, Lin X, Wang Y L, Du S and Gao H J 2019 *Chin. Phys. B* **28** 056801
[11] Xia B, An L, Gao D, Shi S, Xi P and Xue D 2015 *CrystEngComm* **17** 6420
[12] Withers F, Del Pozo-Zamudio O, Schwarz S, Dufferwiel S, Walker P M, Godde T, Rooney A P, Gholinia A, Woods C R, Blake P, Haigh S J, Watanabe K, Taniguchi T, Aleiner I L, Geim A K, Fal'ko V I, Tartakovskii A I and Novoselov K S 2015 *Nano Lett.* **15** 8223
[13] Zhao Y, Bo T, Du L, Tian J, Li X, Watanabe K, Taniguchi T, Yang R, Shi D, Meng S, Yang W and Zhang G 2021 *Chin. Phys. B* **30** 057801
[14] Wang Q H, Kalantar-Zadeh K, Kis A, Coleman J N and Strano M S 2012 *Nat. Nanotechnol.* **7** 699

[15] Manzeli S, Ovchinnikov D, Pasquier D, Yazyev O V and Kis A 2017 *Nat. Rev. Mater.* **2** 17033

[16] Sutter E, Huang Y, Komsa H P, Ghorbani-Asl M, Krasheninnikov A V and Sutter P 2016 *Nano Lett.* **16** 4410

[17] Fan P, Qian G, Wang D, Li E, Wang Q, Chen H, Lin X and Gao H J 2021 *Chin. Phys. B* **30** 018105

[18] Li E, Zhang R Z, Li H, Liu C, Li G, Wang J O, Qian T, Ding H, Zhang Y Y, Du S X, Lin X and Gao H J 2018 *Chin. Phys. B* **27** 086804

[19] Lin J, Zuluaga S, Yu P, Liu Z, Pantelides S T and Suenaga K 2017 *Phys. Rev. Lett.* **119** 016101

[20] Tian Z, Zhao M, Xue X, Xia W, Guo C, Guo Y, Feng Y and Xue J 2018 *ACS Appl. Mater. Interfaces* **10** 12831

[21] Xue M, Zheng Q, Chen R, Bao L, Du S and Chen J 2019 *Nanoscale* **11** 14113

[22] Fang Z, Hao S H, Long L Y, Fang H, Qiang T T and Song Y X 2014 *CrystEngComm* **16** 2404

[23] Pei T, Bao L, Wang G, Ma R, Yang H, Li J, Gu C, Pantelides S, Du S and Gao H J 2016 *Appl. Phys. Lett.* **108** 053506

[24] Pei T, Bao L, Ma R, Song S, Ge B, Wu L, Zhou Z, Wang G, Yang H, Li J, Gu C, Shen C, Du S and Gao H J 2016 *Adv. Electron. Mater.* **2** 1600292